NUMERICAL ALGORITHMS FOR STEADY AND UNSTEADY INCOMPRESSIBLE NAVIER-STOKES EQUATIONS

Final Report
NASA Interchange No. NCA2-210

Mohammed Hafez
Jennifer Dacles

Dept. of Mechanical Engr.
University of California, Davis
Davis,Ca 95616

Numerical Algorithms for Steady and Unsteady Incompressible Navier-Stokes Equations

M. Hafez , J. Dacles
Dept. of Mechanical Engineering
U. C. Davis

Summary

The numerical analysis of the incompressible Navier-Stokes equations are becoming important tools in the understanding of some fluid flow problems which are encountered in research as well as in industry. With the advent of the supercomputers, more realistic problems can be studied with a wider choice of numerical algorithms.

This report presents an alternative formulation for viscous incompressible flows . The incompressible Navier-Stokes equations are cast in a velocity/vorticity formulation (1). This formulation consists of solving the Poisson equations for the velocity components and the vorticity transport equation.

Two numerical algorithms for the steady two-dimensional laminar flows are presented. The first method is based on the actual partial differential equations. This uses a finite-difference approximation of the governing equations on a staggered grid. The second method uses a finite element discretization with the vorticity transport equation approximated using a Galerkin approximation and the Poisson equations are obtained using a least squares method. The equations are solved efficiently using Newton's method and a banded direct matrix solver (LINPACK).

The method is extended to steady three-dimensional laminar flows and applied to a cubic driven cavity using finite difference schemes and a staggered grid arrangement on a Cartesian mesh. The equations are solved iteratively using a plane zebra relaxation scheme.

Currently, a two-dimensional, unsteady algorithm is being developed using a generalized coordinate system. The equations are discretized using a finite-volume approach. This work will then be extended to three-dimensional flows.

Algorithm Development

Background

Some of the widely used solution methods in the study of viscous incompressible flows are the primitive variable formulation for both 2-D and 3-D and the vorticity/stream function for 2-D and plane flows. Under the class of the primitive variable formulations are the artificial compressiblity method as developed by Kwak , et. al. (2) and the fractional step method by Kim,and Moin (3). More recently, Rosenfeld, et. al extended the fractional step method for unsteady 3-D flow problems (4). One of the major concerns about this formulation is the prescription of pressure on the boundary and the method of obtaining the pressure. Mass conservation is an important criterion that must also be satisfied. While the pressure does not explicitly appear in the continuity equation it acts as an important parameter in ensuring that continuity is satisfied. Pressure can be eliminated from the equation by introducing the vorticity/stream function formulation for 2-D . This formulation conserves mass automatically. This method can be extended to 3-D using the vorticity/vector potential method. However, this extension is not straightforward. Vorticity can be eliminated from this equation to obtain a single biharmonic stream function formulation. One of the issues of this formulation is that one may lose accuracy if the formulation is not done correctly. Convergence with this method is also slow.

The velocity/vorticity method is a combination of the primitive variable formulation and the stream function formulation. This method eliminates the problem with the pressure but introduces the problem of the vorticity boundary conditions. Many different techniques to overcome the problem of the vorticity boundary conditions have been presented in the literature. They are grouped into 3 different types of schemes. The first scheme uses the relationship between velocity and stream function.(12,15).
The second class are those proposed by Quartapelle and Quartapelle and Valz-Gris(16,17). These papers showed that in order for the boundary conditions on the velocity be satisfied the vorticity should evolve subject to an integral constraint. The third class of method uses the vortex blob methods as introduced by Chorin. The present treatment of vorticity boundary condition fall under the second class.

The boundary conditions on the velocity induce a constraint on the vorticity. The equation for the definition of vorticity is then solved as part of the flow.

The equations that are being used in this type of approach is of a higher order than the original partial differential equations. Because of this, less restrictive boundary conditions can be used. This may be advantageous for those applications where restrictive boundary conditions are problematic.

Another advantage of this method when used with a staggered mesh arrangement is that it gives a compact and accurate representation of the conservation of mass and vorticity. The natural decoupling of the governing equations is also beneficial since this will lead to simple treatment of the boundary conditions. This method seems favorable for most 2-D flow applications. However, the extension to 3-D may present some drawbacks.

One of the major concern is the increased number of equations and unknowns. You now have three equations for the velocity and three vorticity components. This problem may be alleviated by not solving the equations directly as was done in the 2-D case but rather by using an efficient relaxation which will be competitive with the other formulations. This problem will be addressed later on when the 3-D unsteady formulation using a generalized coordinate system is finished.

Governing Equations

The continuity equation, the definition of vorticity and the vorticity transport equation are given by equations (1)-(3).

$$\nabla \cdot \vec{q} = s \ , \quad \nabla \times \vec{q} = \vec{\omega}$$

$$\frac{D\vec{\omega}}{Dt} = \vec{\omega} \cdot \nabla\vec{q} + \nu\nabla^2\vec{\omega}$$

In equation (1), s represents a source distribution in the field. If $s \neq 0$, then continuity equation cannot be automatically satisfied by introducing a stream function for two dimensional and axisymmetric flows. Moreover, the use of stream functions in multiply connected domains requires special treatment of boundary conditions.

To solve equations (1)-(2), with prescribed normal velocity components on the boundary, Rose (4,5) introduced a compact finite difference scheme which leads to an ill-conditioned system of equations. Osswald, Ghia and Ghia (6) used a direct solver for their discrete velocity equations decoupled from the vorticity equation. Recently Chang and Gunzburger(7) proposed a finite element discretization of equations (1)-(2), which leads to a rectangular algebraic system of equations.

The solution of equations (1),(2), with prescribed normal velocity component on the boundary,exists only if some compatibility relations hold. For example, using Gauss theorem one obtains

$$\iiint_V \nabla \cdot \vec{q} \, dV = \iiint_V s \, dV = \iint_A \vec{q} \cdot \vec{n} \, dA$$

where n is the unit vector perpendicular to A. Similarly, it can be shown that

$$\iiint_V \nabla \times \vec{q} \, dV = \iiint_V \vec{\omega} \, dV = \iint_A \vec{n} \times \vec{q} \, dA$$

Also, the following vector identity must hold

$$\nabla \cdot \nabla \times \vec{q} = \nabla \cdot \vec{\omega} = 0$$

Fasel proposed to take the curl of equation (2)

$$\nabla \times \vec{\omega} = \nabla \times (\nabla \times \vec{q}) = \nabla(\nabla \cdot \vec{q}) - \nabla^2\vec{q}$$

Substituting equation (1) in equation (7) gives

$$-\nabla^2\vec{q} = \nabla\times\vec{\omega} - \nabla s$$

Assuming w is known, the Poisson equations with Dirichlet boundary conditions can be solved for the velocity components. In general, equation (8) admits more solutions than those of equations (1)-(2). For the case of "inviscid" flow, in a simply connected domain, Fix and Rose (8) and Phillips (9) showed that the solution of equations (1) and (2) with prescribed normal velocity components can be obtained as a solution of equation (8). Besides the normal velocity components, equation (2) is used as boundary conditions for equation (8). With this choice, equation (8) has a unique solution, and spurious solutions are excluded.

To extend the above analysis to the viscous flow case, the prescribed velocity at the boundary is decomposed into two sets: the normal and the tangential components. The normal component together with the definition of the vorticity are imposed as boundary conditions for equation (8). The tangential velocity components provide boundary conditions for the vorticity transport equation. If equation (8) and the vorticity transport equation are solved in a coupled manner, there is no need to identify which boundary condition is used for which equation.

A Least Squares Formulation

Consider the functional

$$I = \frac{1}{2}\iiint_V (\nabla\cdot\vec{q}-s)^2 + |\nabla\times\vec{q} - \vec{\omega}|^2 \, dV$$

Minimizing I with respect to q yields

$$\delta I = 0 = \iiint_V (\nabla\cdot\vec{q} - s)\,\nabla\cdot\delta\vec{q} + (\nabla x\vec{q} - \vec{\omega})\cdot\nabla x\delta\vec{q}\ dV$$

$$= -\iiint_V \nabla(\nabla\cdot\vec{q} - s)\cdot\delta\vec{q} + \nabla x(\nabla x\vec{q} - \vec{\omega})\cdot\delta\vec{q}\ dV$$

$$+ \iint_A (\nabla\cdot\vec{q} - s)\,\delta\vec{q}\cdot\vec{n} + (\nabla x\vec{q} - \vec{\omega})\cdot(\vec{n}x\delta\vec{q})\ dA$$

A more detailed analysis of this equation is shown in the Appendix.

Thus, the Euler-Lagrange equation associated with minimizing I is identical to equation (8), provided the boundary terms vanish. The latter condition is satisfied if i) the velocity vector q is specified at the boundary; ii) the tangential velocity components are specified and equation (1) is imposed at the boundary; or iii) the normal velocity component is specified and the tangential components of equation (2) are imposed at the boundary.

Assume the boundary conditions of iii) are used to determine the velocity field. To solve the vorticity transport equations, three boundary conditions are required; these are the two tangential velocity components prescribed at the boundary as well as the compatibility condition on the vorticity field .
It is noticed by Gunzberger and Patterson (10) that the latter is a natural boundary condition associated with the Galerkin formulation of the vorticity transport equation. Moreover, taking the divergence of the vorticity equation, it is shown that $\nabla\cdot\vec{\omega}=0$ is governed by a linear homogeneous equation and hence $\nabla\cdot\vec{\omega}$ vanishes everywhere.

To avoid the coupling between the velocity components at the curved boundaries, the boundary condition i) may be used instead, to determine the velocity field. The boundary conditions for the vorticity transport equations are still

$$\vec{\omega}x\vec{n} = \nabla x\vec{q}x\vec{n}. \quad \text{and} \quad \nabla\cdot\vec{\omega} = 0$$

Special treatment may be required, however, to determine accurately the tangential vorticity component at a curved boundary in terms of the derivatives of the velocity components.

Numerical Techniques and Discretization

Finite Difference Discretization.

The terms are discretized using central difference schemes and staggered grid formulation. This formulation defines vorticity to be in the center of the grid while the velocity components are located along the edges. The extension of this approach to 3-D schemes is also applied. The method of solution is as follows: For the 2-D formulation, the equations are solved fully coupled using Newton's method of linearization and a direct solver package (LINPACK) . An outline of what subroutines are called and their roles are given in the Appendix. For the 3-D formulation, the Poisson equations are solved directly. The LU decomposition for the velocity components are only done once and can be stored for later use. This will help with the cpu requirement. The vorticity transport equations are solved using a zebra line relaxation method for each of the 3 planes. The 2-D staggered grid arrangement is show in Fig. 1 while the 3-D arrangement is show in Fig. 2.

Finite Element Discretization.

A discrete approximation of the functional I can be easily constructed using finite element techniques. Using standard bilinear shape functions for the velocity components, the functional I can be evaluated in terms of the nodal values. Upon minimization over each element and assembling the contribution from all elements, the nodal equations are readily obtained.
A Galerkin method due to Swartz and Wendroff (11) (see also Fletcher (12)) is used for the vorticity equation. The boundary conditions are implemented as discussed before. There resulting nonlinear system of algebraic equations are solved by Newtons method and a direct solver.

For a simple geometry, a finite difference discretization over a staggered grid leads to the five point stencil for the Poisson equations. The stencil for the finite element method is shown in Fig. 1.

Finite Volume Discretization (Generalized Coordinate System).

When arbitrary geometries are considered the choice of the discretization scheme is crucial. The discretized governing equations and their compatibility relations must be satisfied as well a certain geometrical identities when a generalized coordinate system is employed. The finite-volume approach can give accurate conservative approximations as was pointed out by Vinokur (13). This method was also appled by Rosenfeld et al (14) using a primitive variable formulation on a staggered mesh and a generalized non-orthogonal system using the velocity/vorticity formulation.

The choice of the dependent variables is also critical in obtaining the accurate solutions. The scaled contravariant velocity components in a staggered grid arrangement are used as the dependent variables instead of the conventional Cartesian velocity components. This choice is essential for mass conservation on the discrete level.

The Integral Formulation of the Governing equations are:

$$\iint \mathbf{q} \cdot \mathbf{n}\, dS = 0 \qquad \text{(mass conservation)}$$

$$\iint \mathbf{n} \times \mathbf{q}\, dS = \iiint \boldsymbol{\omega}\, dV \qquad \text{(definition of vorticity)}$$

$$\iint \boldsymbol{\omega} \cdot \mathbf{n}\, dS = 0 \qquad \text{(conservation of vorticity)}$$

$$\iint (\nabla \mathbf{q}\, \mathbf{n} + \mathbf{n} \times \boldsymbol{\omega})\, dS = 0$$

$$\iint (\mathbf{n}\, \mathbf{q}\, \boldsymbol{\omega} - \mathbf{n}\, \boldsymbol{\omega}\, \mathbf{q} - \mathbf{n}\, \boldsymbol{\omega})\, dS = 0$$

The geometric identity

$$\iint \mathbf{n} dS = 0$$

imposes the condition that the cell is closed. Another conditon that must be also satisfied is that the sum of the cell volumes must equal the total
volume of the flow region.

These conditions are automatically satisfied for the special case of staggered Cartesian coordinates for a cubic driven cavity.

Numerical Results

The flow over a backward facing step is simulated using exactly the same geometry as Ref. 2. The domain of integration is bounded by solid surfaces at the top and the bottom of the backward facing step. At the inlet station, a parabolic velocity profile is imposed between the shoulder and the upper surface and it is assumed that the flow is parallel(i.e. the upstream effect of the shoulder is neglected). At the exit, the flow is assumed to be fully developed (independent of x) ,and so v=0. The tangential velocity component (u) is not known and the continuity equation is enforced at the exit boundary. Fig. 3 shows the problem formulation for this case.
Fig. 4 shows the computing time for the Cray X-MP as compared to the INS3D code and the fractional step method. The streamlines are plotted in Figures 5-8 for the Reynolds number ranges of 133 through 1867.

Experimental resuts not only gave the expected primary zone of recirculation region attached to the step but also showed additional recirculation region downstream of the steps and on both sides of the channel. Experiments have shown that transition to turbulence happens at around RE=900. This means that the laminar and steady flow assumption that was mentioned earlier is no longer valid. However, much higher Reynolds number are analyzed to show that the method is robust. Fig. 11 shows the convergence history for both

finite difference and finite element formulation. Quadratic convergence is obtained independent of the grid size and Re provided the initial guess is available. Comparison with other numerical results and experimental data are also given. Mesh refinement is also performed and it is seen that the finite element results are less sensitive to the grid size.

Fig. 12 shows the convergence history for the 3-D driven cavity problem.
The domain is bounded by solid surfaces everywhere with the top wall moving at a uniform velocity of U=1 in the positive x - direction.

Grid sizes of 9x9x9 up to 17x17x17 are used for Re=100. These conditions are chosen to obtain direct comparison with the published results. Figure 13 shows the distribution of the u-velocity component along the centerline(z=0.5,y=0.5,x=0.5) as compared with numerical results obtained by Dennis et. al.

Figure 14 shows the variation of the velocity component as a function of y at z=0. and x=0.5 as compared with Dennis et al.

The vorticity contours compare well with Osswald et al for the same grid size of 17x17x17. The contours for station x=0.5,y=0.5,z=0.5 are shown in Fig 15 while the contours for station x=0.71785,y=0.71785,z=0.71785 are show in Fig. 16.

The current work is on 2-D unsteady flow around a cylinder using curvilinear coordinates.

References

1. Fasel , M. J. F. M. Vol 78, pp 355-383, 1976.
2. Kim, J. and Moin, P. J. of Comp. Physics, Vol 59, No. 2, pp 308-323, 1985.
3. Armaly, B. et. al. J.F. M. Vol 127, 1983.
4. Rose, M., SIAM J. Numer. Analysis, Vol 18, No. 2 1981.
5. Gatski, T., Grosch, C. and Rose M., J. of Comp. Phys. , Vol 48, No. 1, 1982.
6. Osswald, G., Ghia K. and Ghia, U. AIAA paper, 87-1139.
7. Chang,C. and Gunzberger, M., 1988.
8. Fix, G. and Rose, M., SIAM J. Numer. Analysis Vol 22. No. 2, 1985.
9. Phillips, T. , IMA J. of Num. Analysis , Vol 5. 1985.
10. Gunzberger, M. and Peterson, J. 1988.
11. Swartz, B. and Wendoff, B. Math of Comp. Vol 23, 1969.
12. Fletcher, C. J. of Comp. Phys. Vol 51, 1983.
13. Rogers, S. , Kwak, D. ,Chang, J. NASA TM 86840.
14. Dennis, S. Ingham D., Cook, R. "Finite-Difference Methods for Calculating Steady Incompressible Flows in Three Dimensions". J. of Comp. Physics. 1979.
15. Hafez, M. , Dacles, J. , Soliman, M. " A Velocity/Vorticity Method for Viscous Incompressible Flow Calculations", Lecture Notes in Physics Vol 323,1986.
16. Rosenfeld, M. Kwak, D. and Vinokur M. " A Solution Method for the Unsteady and Incompressible Navier-Stokes Equations in Generalized Coordinate Systems, AIAA paper, 88-0718.
17. Vinokur, M. "An Analysis of Finite-Difference and Finite-volume Formulations of Conservation Laws", NASA CR-177416, 1986.
18. Quartapelle L., Valz-Gris, Int. J. Numer. Math. Fluids 1,1129 (1981).
19. Quartapelle L., J. Comput. Phys. 40, 453 (1981).
20. Anderson, C., J. Comp. Physics, 80, 72-97, 1989.

Discretization

Finite difference: -discretize by central difference
-staggered grid

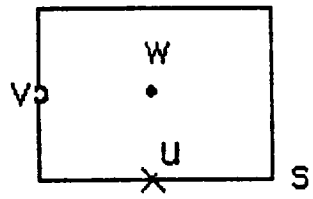

w=vorticity
u,v=vel comp
$s = u_x + v_y$

Finite Element : -discretize using bilinear shape functions
-regular grid

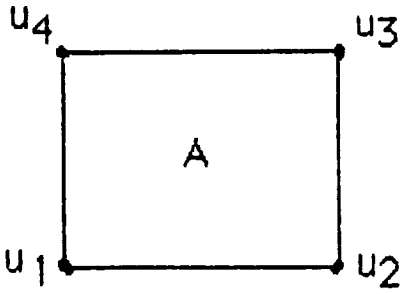

$$u_i(x,y) = a_{u_i} + b_{u_i} x + c_{u_i} y + d_{u_i} xy$$

Figure 1.

Proposed Method for 3-D Velocity-Vorticity Formulation

Governing equations (3-d)

(11) $u_{xx} + u_{yy} + u_{zz} = (w_2)_z - (w_3)_y$

(12) $v_{xx} + v_{yy} + v_{zz} = (w_3)_x - (w_1)_y$

(13) $w_{xx} + w_{yy} + w_{zz} = (w_1)_y - (w_2)_x$

(14) $u(w_1)_x + v(w_1)_y + w(w_1)_z - w_1 u_x - w_2 u_y - w_3 u_z = \frac{1}{Re}[w_{1xx} + w_{1yy} + w_{1zz}]$

(15) $u(w_2)_x + v(w_2)_y + w(w_2)_z - w_1 v_x - w_2 v_y - w_3 v_z = \frac{1}{Re}[w_{2xx} + w_{2yy} + w_{2zz}]$

(16) $u(w_3)_x + v(w_3)_y + w(w_3)_z - w_1 w_x - w_2 w_y - w_3 w_z = \frac{1}{Re}[w_{3xx} + w_{3yy} + w_{3zz}]$

(17) $w_1 = w_y - v_z$

(18) $w_2 = u_z - w_x$

(19) $w_3 = v_x - u_y$

3-D staggered grid arrangement:

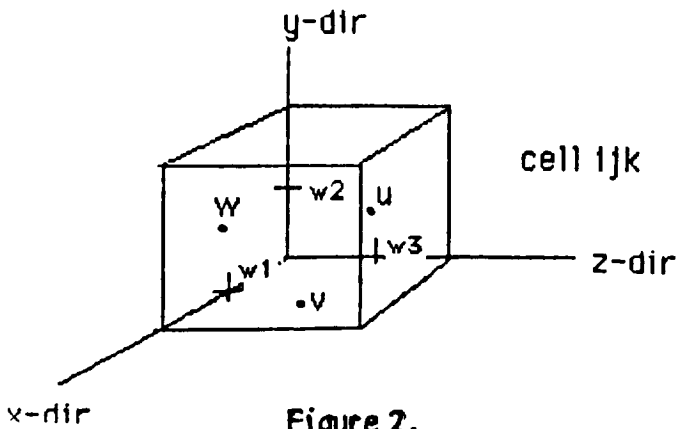

Figure 2.

Problem Formulation (2-D)

(8) $\nabla^2 u = - w_y$

(9) $\nabla^2 v = w_x$

(10) $(uw)_x + (vw)_y = \frac{1}{Re} (w_{xx} + w_{yy})$

non-dimensionalized variables :

$x = x'/h$, $y = y'/h$, $u = u'/Umax$, $v = v'/Umax$

$w = w'/(Umax/h)$, $Re = \frac{(2/3)Umax(2h)}{\nu}$

Umax = maximum inlet velocity
h = step height
L = channel length
ν = kinematic viscosity

Test model (2-D backward facing step) :

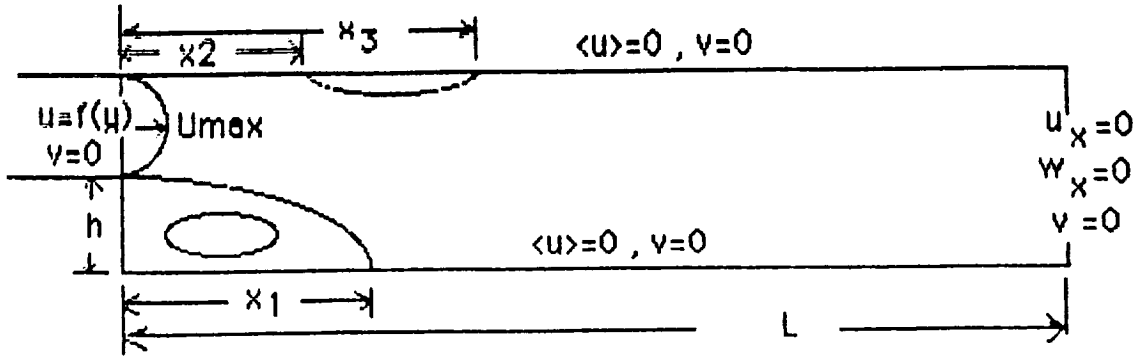

Figure3

COMPUTING TIME FOR BACKWARD FACING STEP
ON CRAY X-MP

(T= t cpu sec/grid point /iteration)

Re	INS3D	FRACTIONAL STEP	PRESENT METHOD
100.	2.0 x10-6	1.5 x10-6	*cpu time range of
200.	2.0 x10-6	3.1 x10-6	1.5 x10-6 to 3.0 x10-6
300.	2.6 x10-6	5.2 x10-6	for Re=100 to 1800
400.	6.7 x10-6	8.2 x10-6	
500.	1.0 x10-5	1.1 x10-5	
600.	1.0 x10-5	1.2 x10-5	
700.	.97 x10-5	1.3 x10-5	
800.	1.0 x10-5	1.4 x10-5	

INS3D and Fractional Step data obtd. from S.Rogers,D.Kwak,J.Chang, Numerical Solution of Incompressible NS Eqns in 3-D General Curvilinear Coord. (NASA TM 86840). Jan 1986

Figure 4.

staggered grid formulation

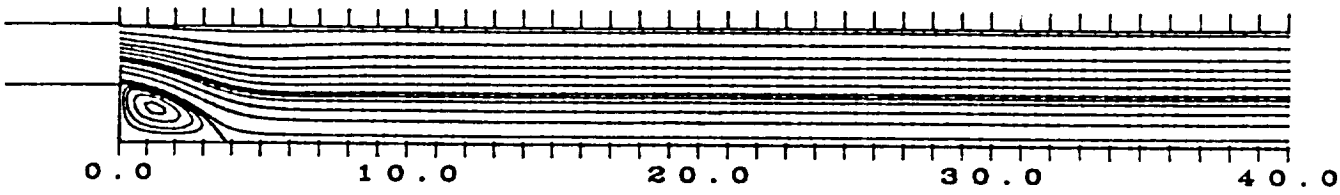

STREAMLINE CONTOURS 105x31

Re=133.

finite element formulation

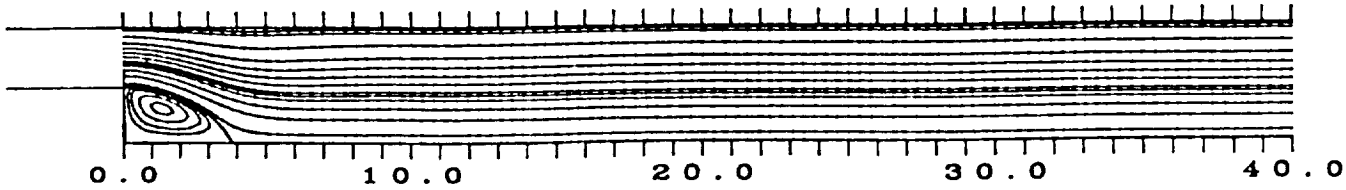

STREAMLINE CONTOURS 105x31

Figure 5

staggered grid formulation

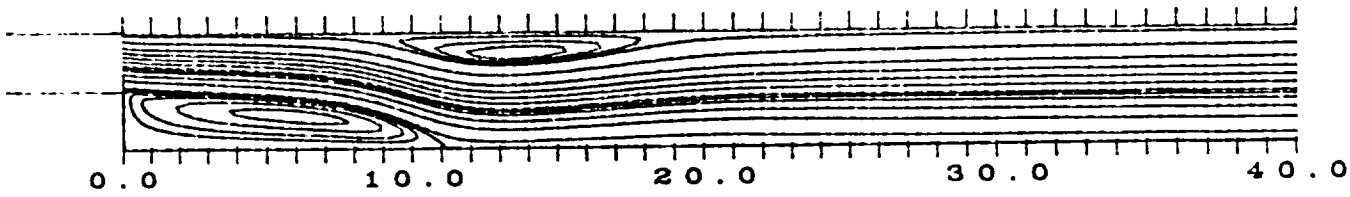

STREAMLINE CONTOURS 105x31

Re= 600.

finite element formulation

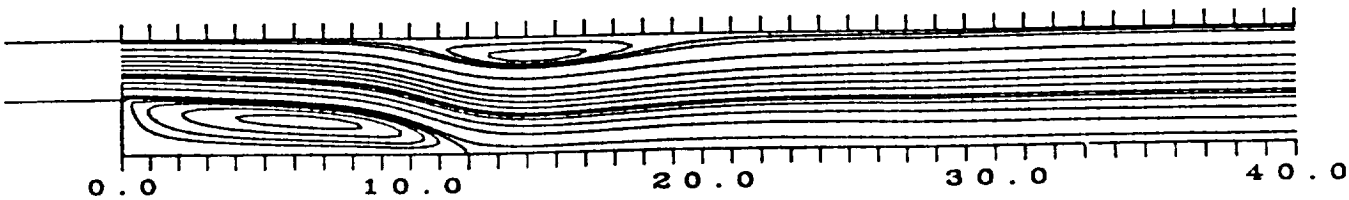

STREAMLINE CONTOURS 105x31

Figure 6.

staggered grid formulation

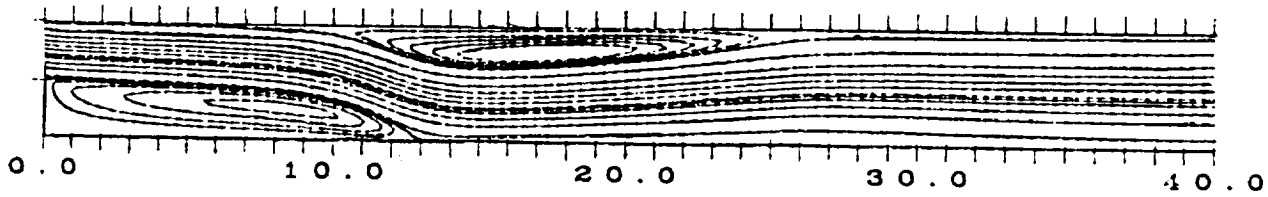

STREAMLINE CONTOURS 105x31

Re=1200.

finite element formulation

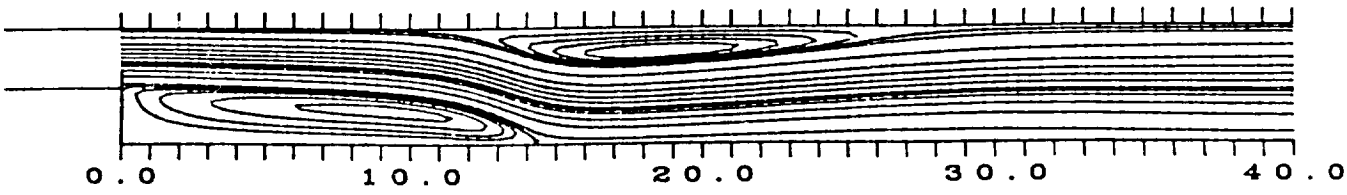

STREAMLINE CONTOURS 105x31

Figure 7.

staggered grid formulation

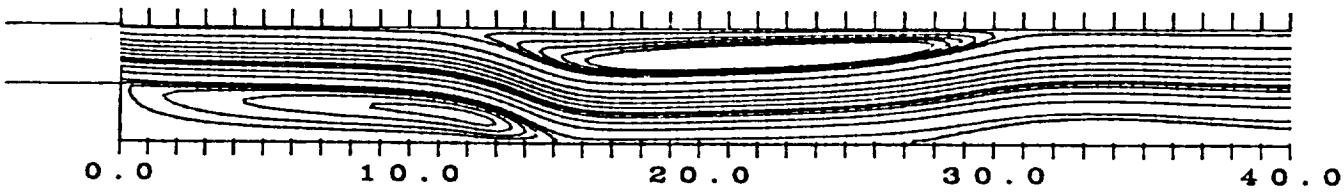

STREAMLINE CONTOURS 105x31

Re=1867.

finite element formulation

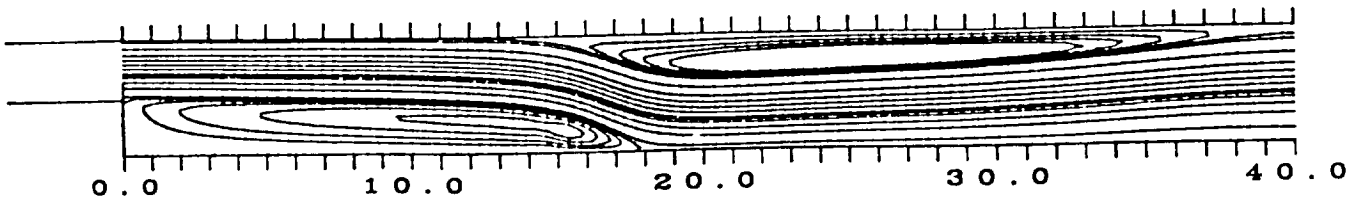

STREAMLINE CONTOURS 105x31

Figure 6.

REATTACHMENT LOCATION OF PRIMARY BUBBLE VS. RE

MESH REFINEMENT

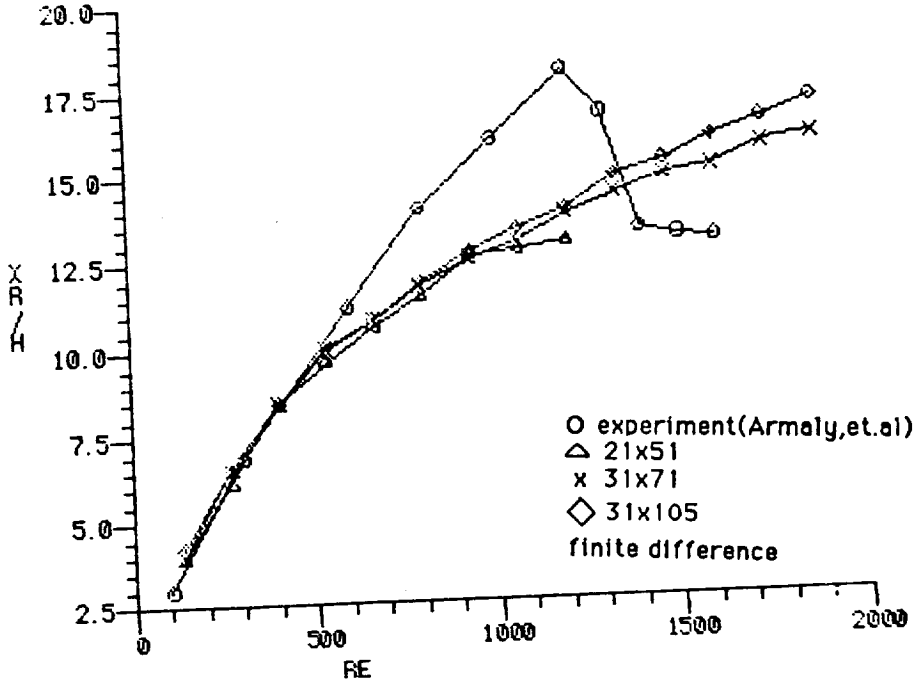

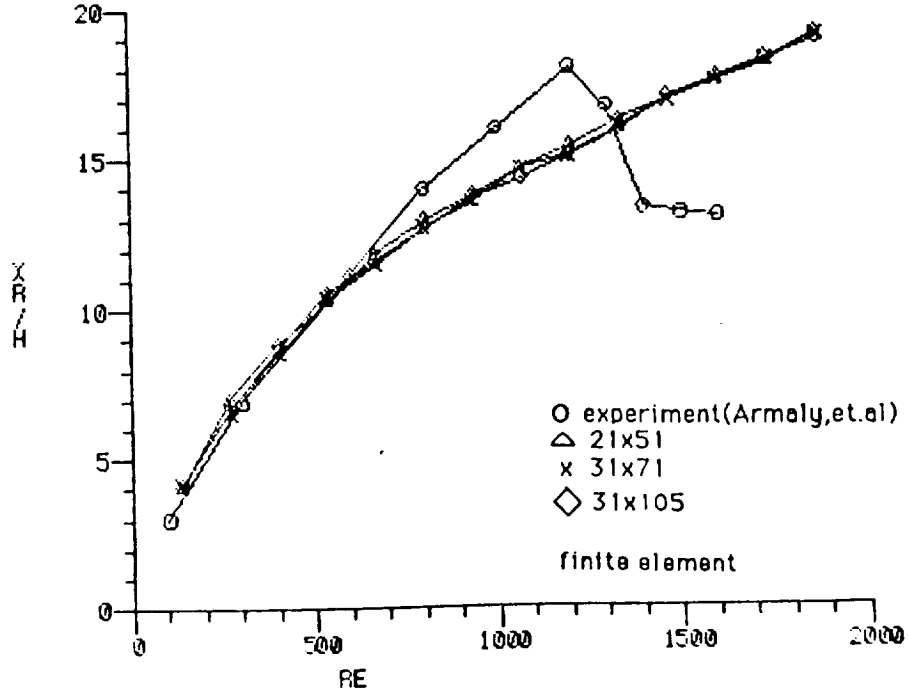

Figure 9

LOCATION OF SECONDARY BUBBLE VS. RE

MESH REFINEMENT

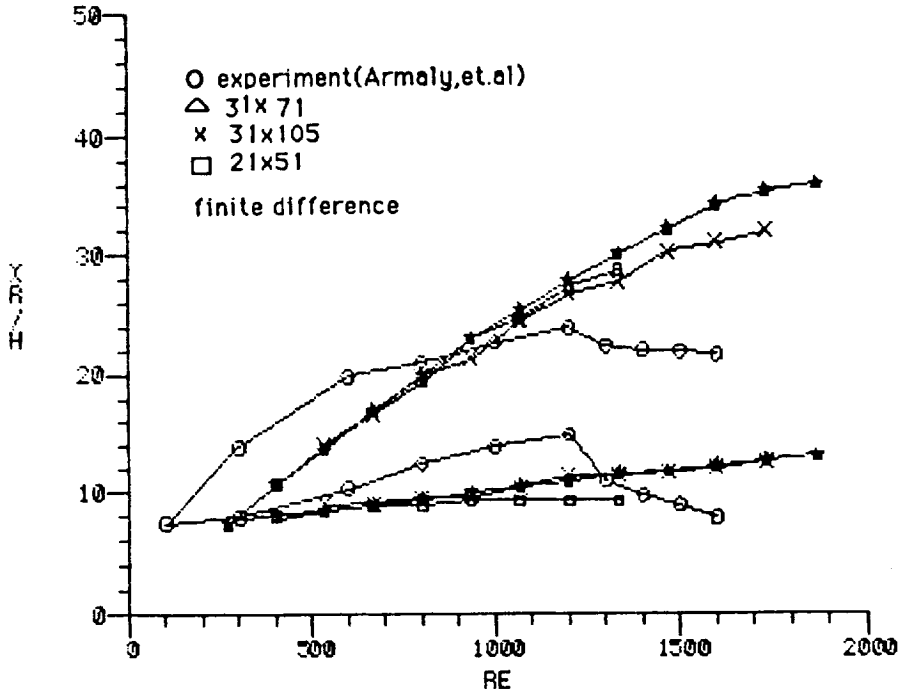

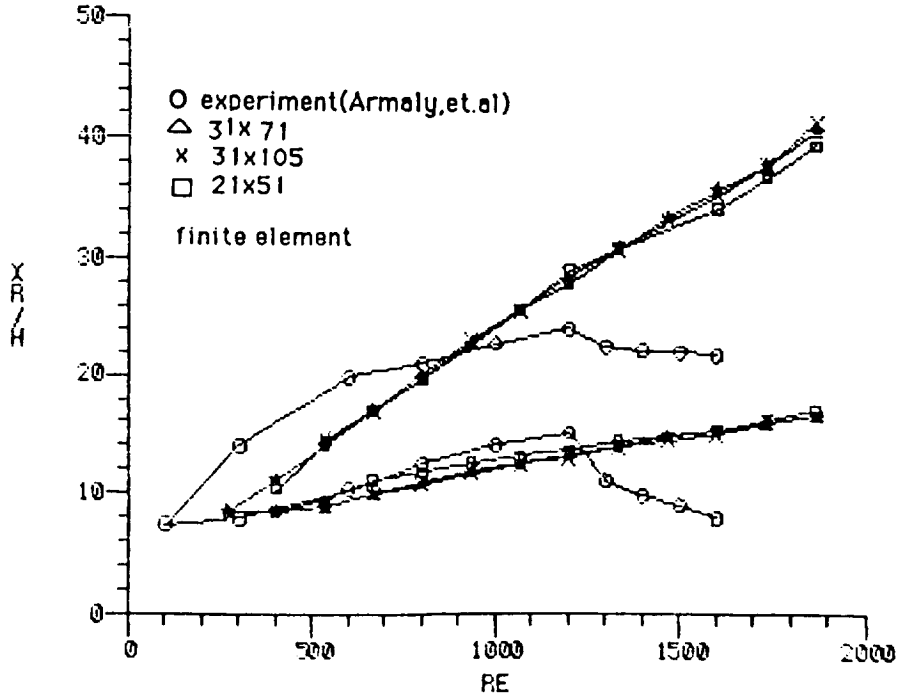

Figure 10.

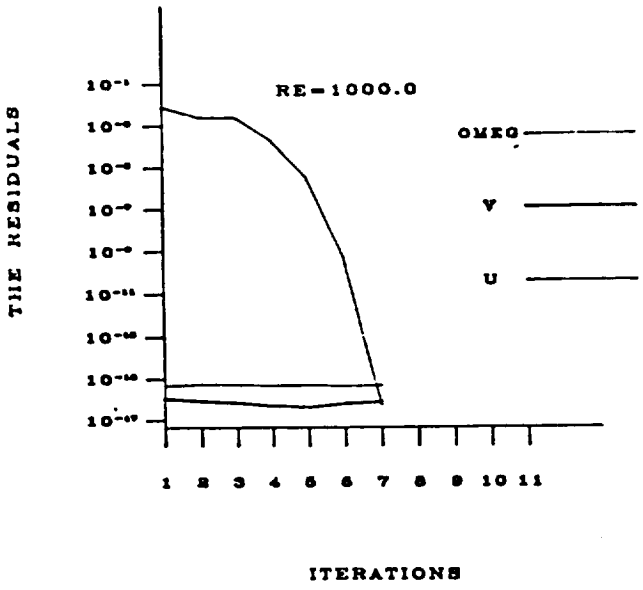

Convergence history of
a finite element calculation

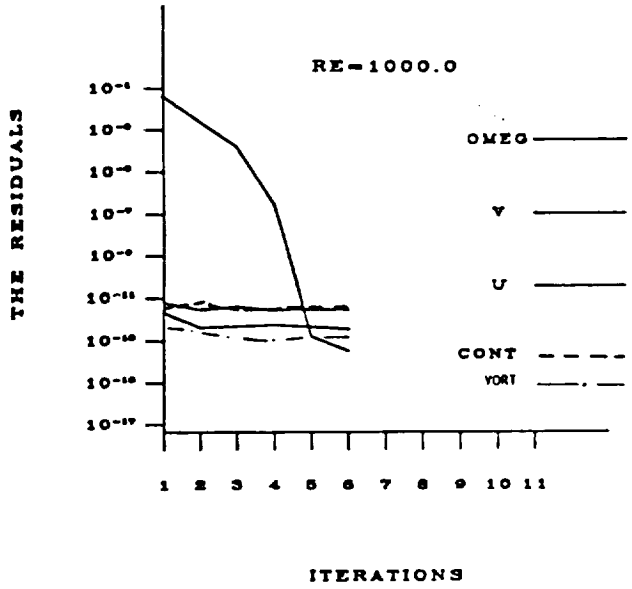

Convergence history of
a finite difference calculation

Figure 11

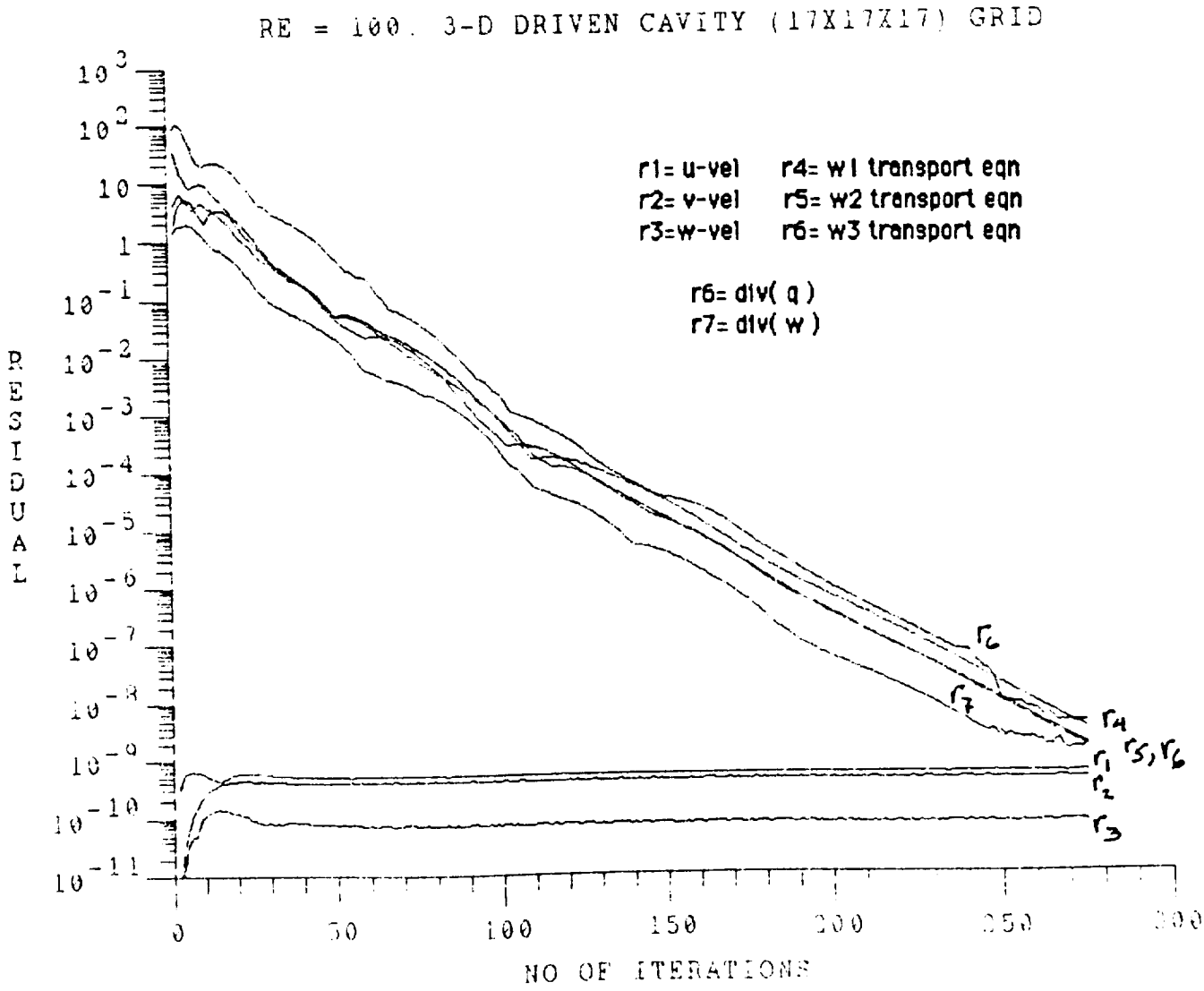

Figure 12. Convergence History

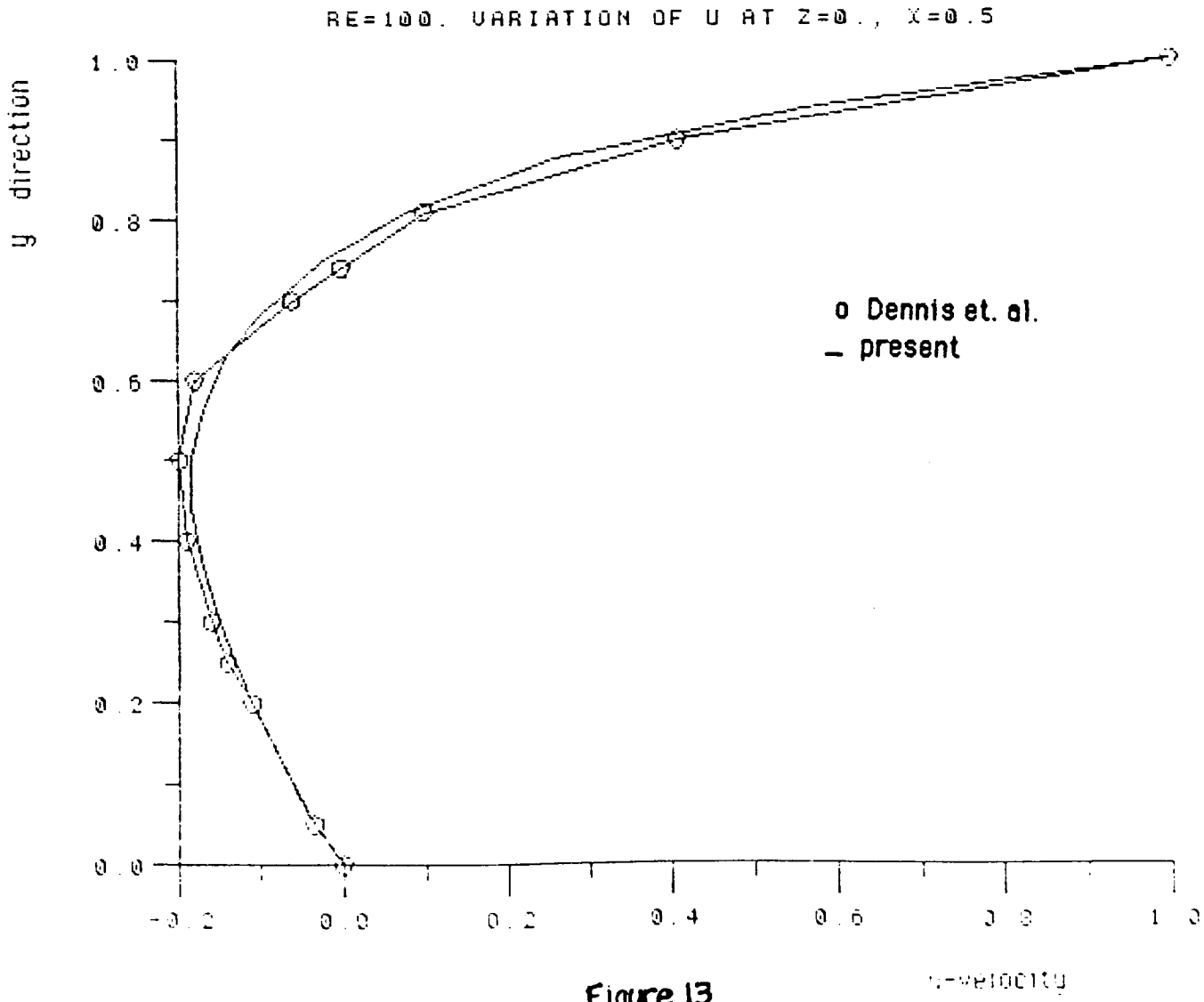

Figure 13

ORIGINAL PAGE IS
OF POOR QUALITY

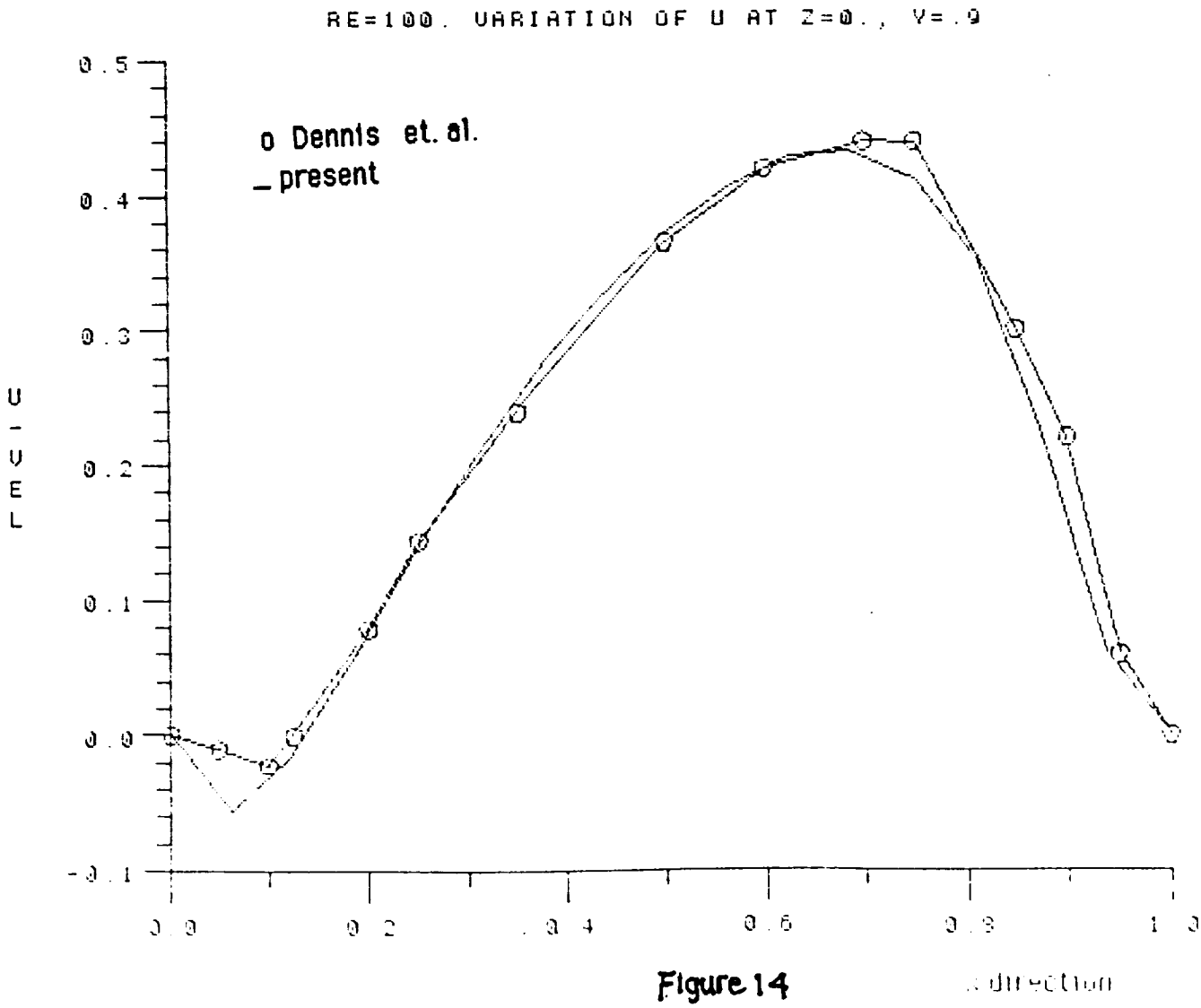

Figure 14

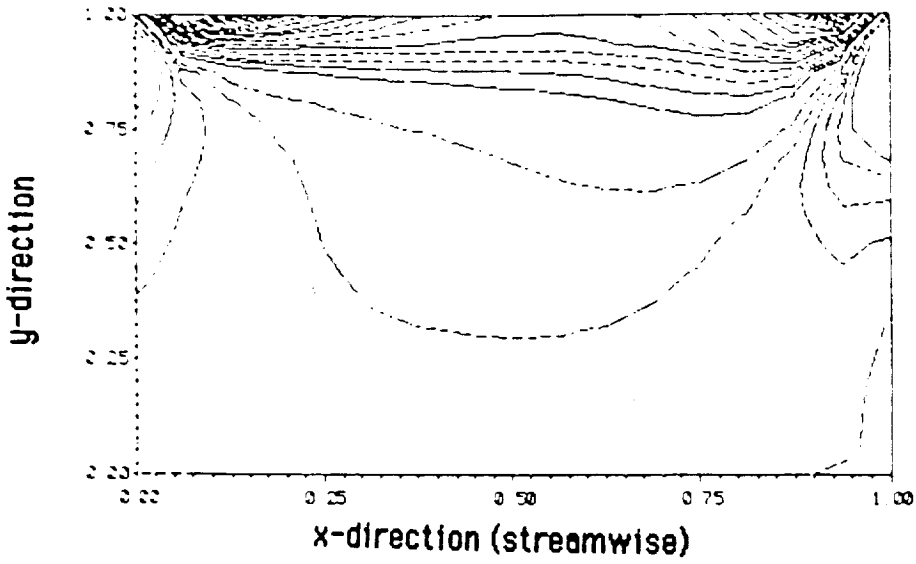

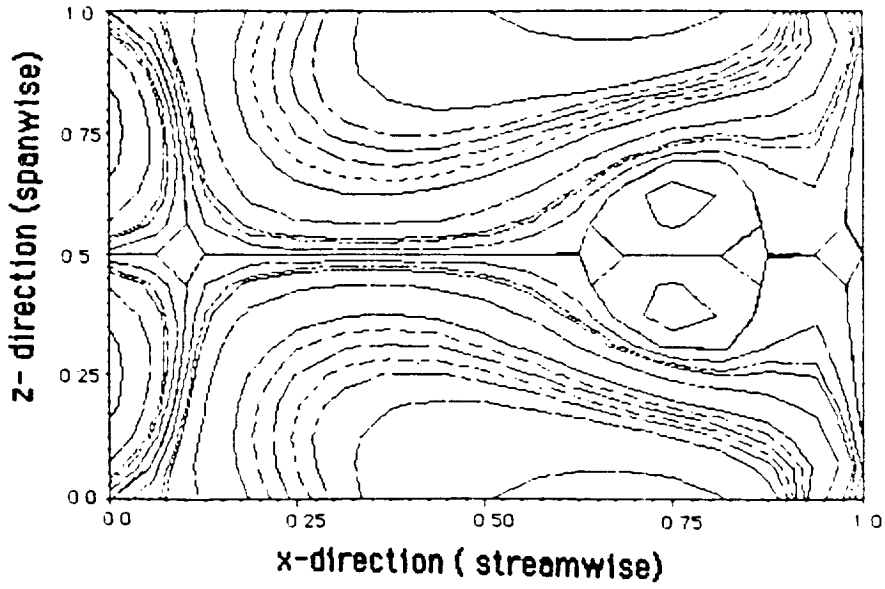

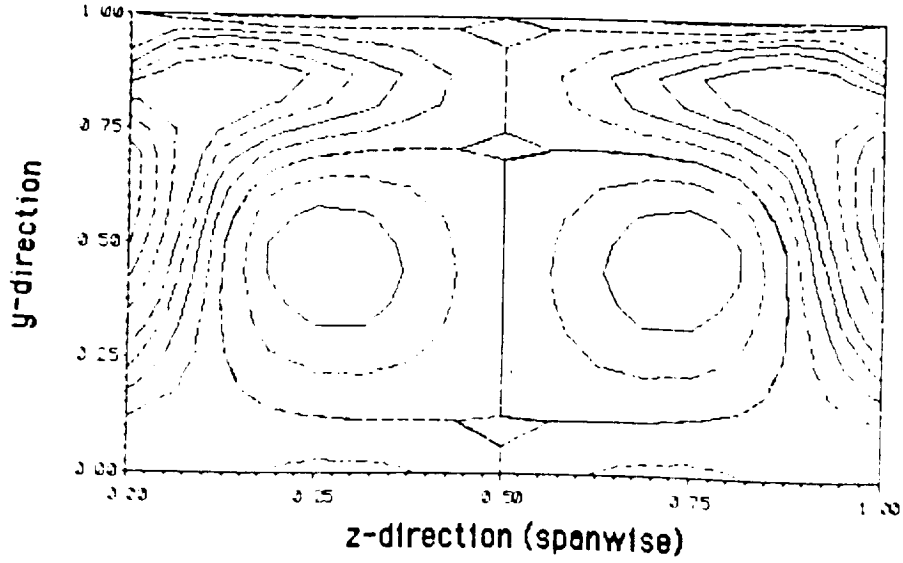

Figure 15 Contours of Normal Vorticity Components at Midplanes
(x=0 , y= 0 , z=0)

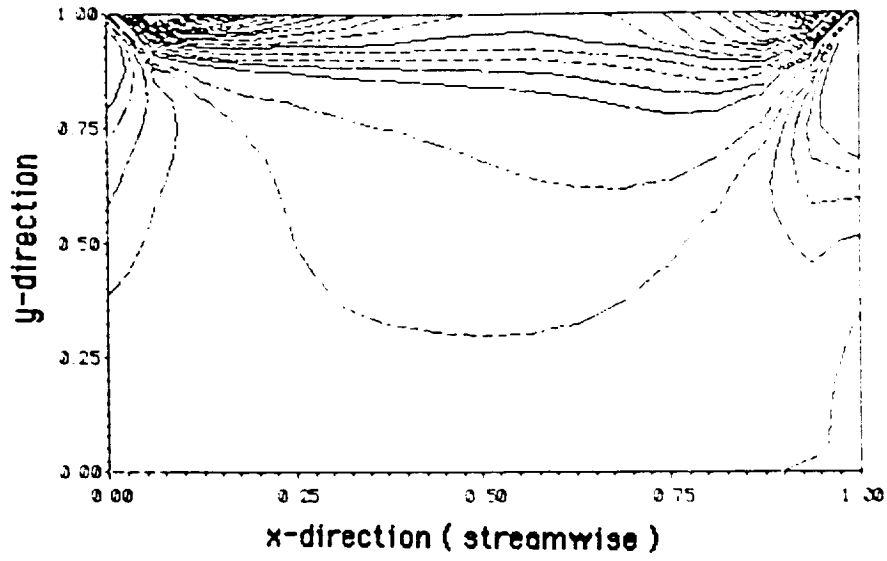

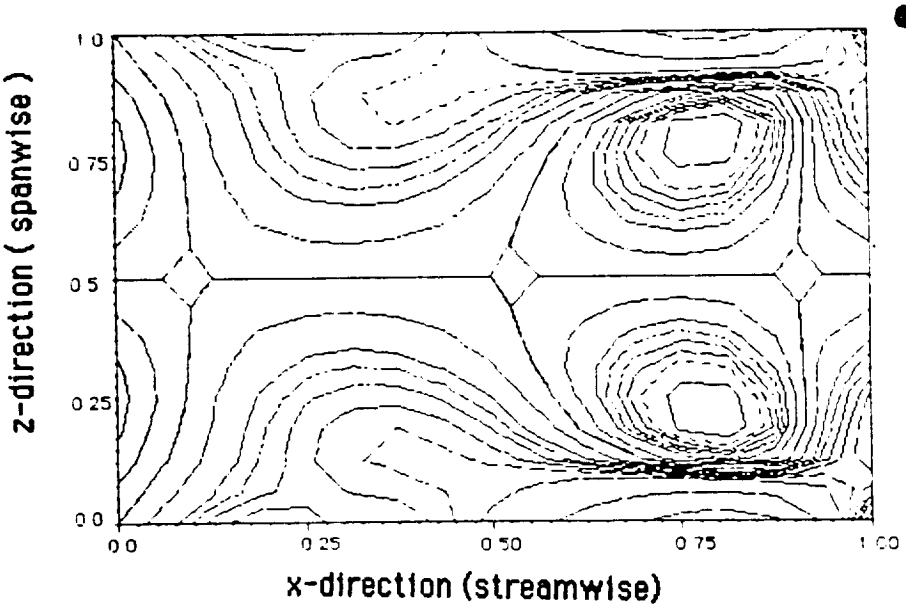

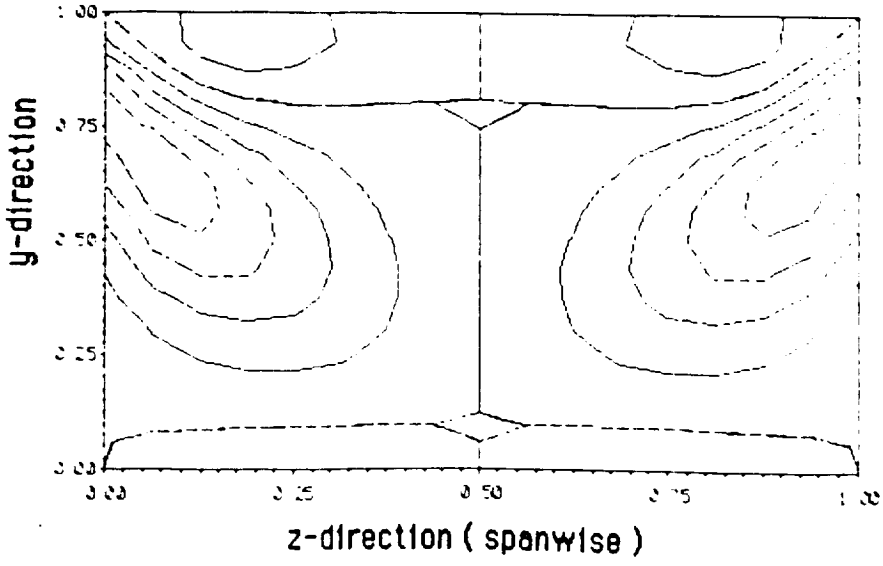

Figure 16 Contours of Normal Velocity Components at (x= 0.71875, y=0.71875, z=0.71875)